Int. J. Multiphase Flow, Vol. 4, pp. 575–583. Pergamon/Elsevier, 1978. Printed in Great Britain

BRIEF COMMUNICATION

PRESSURE DROPS DUE TO PIPE BENDS IN AIR–SOLIDS TWO PHASE FLOWS; CIRCULAR AND ELLIPTICAL BENDS

Y. MORIKAWA, Y. TSUJI, K. MATSUI† and Y. JITTANI
Department of Mchanical Engineering for Industrial Machinery, Osaka University, Suita, Osaka, Japan

(*Received* 23 *May* 1978)

1. INTRODUCTION

Since the design of pneumatic transport equipment requires a correct estimate of the pressure drop at pipe bends, many investigations have been made of this configuration. This work deals with the case of a bend having a form of a quarter ellipse as shown in figure 1.

When the elliptical bend replaces a circular bend with a long sweep at the upstream and a short radius at the downstream end, one expects that erosion per unit surface is reduced (Zenz & Othmer 1960). The reason is that impact points of particles against the pipe wall are distributed over a wider area compared with the circular bend. However, information about the pressure drop due to the elliptical bend are unavailable, not only in two-phase flows but also in single phase flows. Therefore, the pressure drops due to the elliptical bends of different sizes and shapes were measured in the present work. To investigate the relationship between the elliptical and circular bends, measurements were made also for the circular bend. From those measurements, an empirical formula predicting the pressure drop is proposed.

2. EXPERIMENTAL ARRANGEMENT

A suction type of pneumatic conveying system, shown in figure 2, was used. A blower 7, installed after a cyclone separator 6, drew the air–solids mixture through the pipe line. The internal diameter of the test pipe, D, was 40 mm. The bend 4 is made of vinyl chloride. Table 1 shows the dimensions of the bends used in this experiment. The straight pipes in the upstream

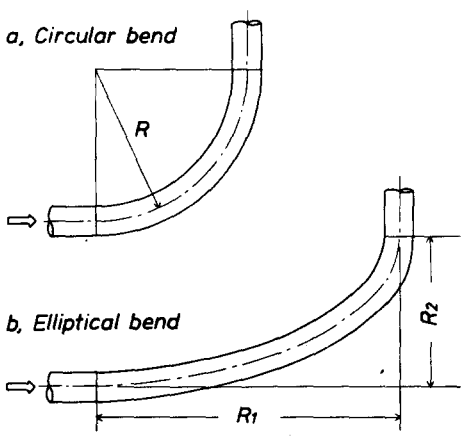

Figure 1. Circular and elliptical bends.

†Present address: Kobe Steel Ltd., Kobe, Japan.

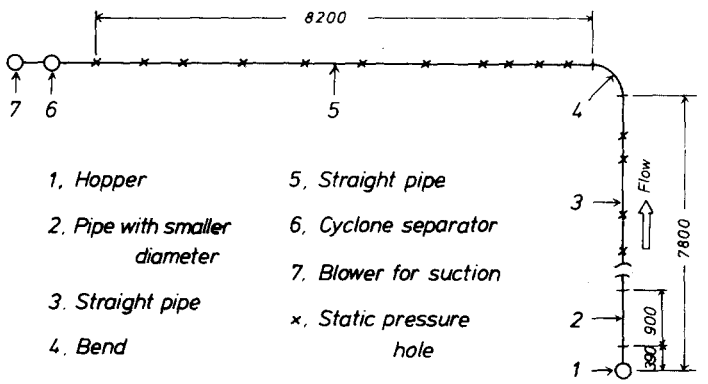

Figure 2. Schematic of the experimental apparatus, plane view.

Table 1. Dimensions of the bend. R_1 and R_2 are defined in figure 1.

Number	Shape	Curvature ratio at the upstream R_1/r	Curvature ratio at the downstream R_2/r	Bend length L_f	Average curvature ratio $\frac{\bar{R}}{r}=\frac{L_f}{r}\Big/\frac{\pi}{2}$
1	circular	12.3		386	
2		20.5		644	
3		28.2		880	
4		36.1		1131	
5	elliptical	6.0	12.2	298	9.5
5′		12.2	6.0		
6		12.1	18.0	488	15.5
6′		18.0	12.1		
7		10.2	20.3	499	15.9
7′		20.3	10.2		
8		12.0	24.5	596	19.0
8′		24.5	12.0		
9		20.6	30.8	815	25.9
9′		30.8	20.6		
10		20.3	41.0	1008	32.1
10′		41.0	20.3		

and downstream of the bend were acrilic and 6.5 m and 8.2 m in length, respectively. Great care was taken to make a smooth connection between the bend and straight pipes sections. Numerous static pressure holes were provided in the straight pipes.

The solid particles used were nearly spherical polyethylene pellets with mean diameter of 1.1 mm and density of 923 kg/m^3. The particles were supplied to the pipe through an electromagnetic feeder, 1. The rate at which the particles fell into air stream was controlled by adjusting the voltage. First, the particles passed through the pipe with 35 mm internal diameter and 900 mm length. This small-sized pipe was used to accelerate the particle velocity more effectively. After passing through this pipe, the particle velocity became constant before the bend. This was inferred from the static pressure distribution along the flow.

In the downstream straight pipe, static pressure measurements were made up to the distance of $240D$ from the end of the bend. This distance was not sufficient to gain a region of completely constant particle velocities. However, in this work, the particle velocity in the most downstream measuring section was approximated to be constant.

The static pressure was measured by an inclined multi-tube manometer. The air flow rate was measured by traversing a Pitot tube in the straight pipe before the particle feeder. The mean air velocity u, ranged from 18 to 29 m/s, and the solids–air loading ratio n, up to 8.

3. DEFINITION OF PRESSURE DROP AND ITS COEFFICIENT

Figure 3 shows an example of measurements for the static pressure distribution, where a measurement at no-loading conditions is also given for comparison. After the particles from the feeder are sufficiently accelerated by the air stream, the static pressure shows a constant gradient which corresponds to the constant particle velocity. A–B in figure 3 indicates such a region. The particles decelerated in the bend are accelerated again in the straight pipe in the same way, and the particle velocity becomes constant after D. When the total pressure drop per unit length ΔL in the straight pipe is denoted by Δp, the drop Δp is considered to have two components, i.e. Δp_a, the pressure drop due to the air, and Δp_s, the additional drop due to the particles,

$$\Delta p = \Delta p_a + \Delta p_s. \qquad [1]$$

When solids loading is not too high, the pressure drop Δp_a is assumed to be equal to the pressure drop which would occur if the air is flowing alone at the same condition. The coefficient of pressure drop due to the air is defined usually as

$$\lambda_a = \frac{\Delta p_a}{\Delta L} \Big/ \frac{\rho u^2}{2D}, \qquad [2]$$

where ρ is the air density. The coefficient λ_a depends on the Reynolds number $Re = uD/\nu$, and the following empirical formulae are applicable (Schlichting 1968).

$$\lambda_a = 0.3164/Re^{0.25}, \quad (10^3 < Re < 10^5) \qquad [3]$$

and

$$\frac{1}{\sqrt{\lambda_a}} = 2.0 \log (Re\sqrt{\lambda_a}) - 0.8. \qquad [4]$$

In analogy of [2], the coefficient of additional pressure drop is defined as

$$\lambda_s = \frac{\Delta p_s}{\Delta L} \Big/ \frac{\rho u^2}{2D}. \qquad [5]$$

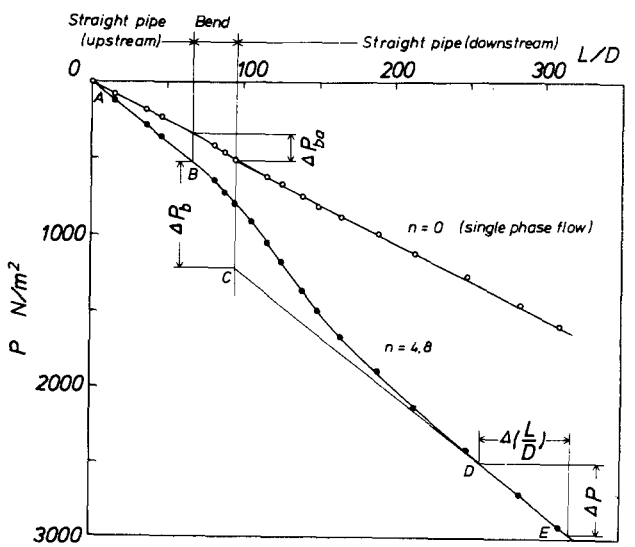

Figure 3. Static pressure distribution along the flow, bend 4, u = 22 m/s.

Generally, the coefficient λ_s depends on the properties of the particles and the pipe, and thus the similarity law of λ_s is not so clear as for λ_a.

The pressure drop due to the bend, Δp_b is defined by the pressure difference shown in figure 3. This pressure drop is also attributed partly to the air and partly to the particles. Then,

$$\Delta p_b = \Delta p_{ba} + \Delta p_{bs}. \qquad [6]$$

The coefficients of pressure drop due to the bend are defined as follows,

$$\zeta_a = \Delta p_{ba} \Big/ \frac{1}{2}\rho u^2 \qquad [7]$$

and

$$\zeta_s = \Delta p_{bs} \Big/ \frac{1}{2}\rho u^2. \qquad [8]$$

Itō (1960) gave empirical formulae for the coefficient ζ_a from an experiment using water flow. His formulae are rewritten for the case of 90° bend as follows,

$$\begin{aligned} \zeta_a &= 0.248\alpha(R/r)^{0.9}/Re^{0.2}, \quad && Re(r/R)^2 < 91 \\ \zeta_a &= 0.217\alpha(R/r)^{0.84}/Re^{0.17}, \quad && Re(r/R)^2 > 91, \end{aligned} \qquad [9]$$

where R is the curvature of the bend, r is $D/2$, and

$$\begin{aligned} \alpha &= 0.95 + 17.2(R/r)^{-1.96}, \quad && R/r < 19.7 \\ \alpha &= 1, && R/r > 19.7. \end{aligned}$$

4. PRESSURE DROP DUE TO THE AIR ALONE

In a preliminary experiment, agreement between measurements and [3] or [4] were confirmed. In this section, the pressure drops due to the bend are shown.

The present results for the circular bend agree with Itō's formulae satisfactorily as shown in figure 4. The results for the elliptical bend are compared with his formulae in figure 5, where the

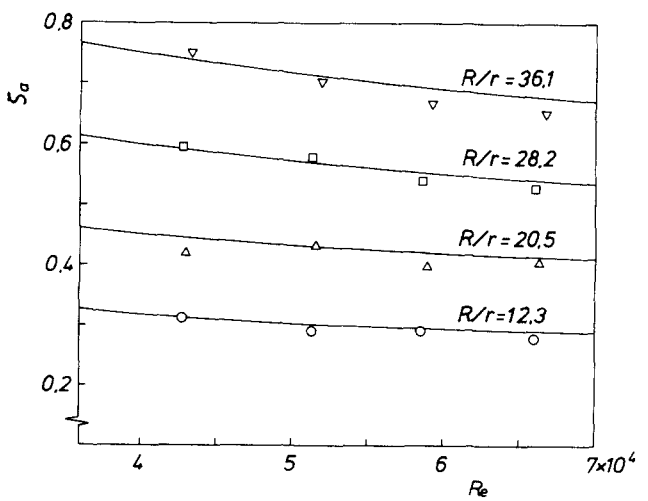

Figure 4. Coefficient of pressure drop due to the circular bend. ○, Bend 1; △, bend 2; □, bend 3; △, bend 4; measurements. ——, Itō's formula[9].

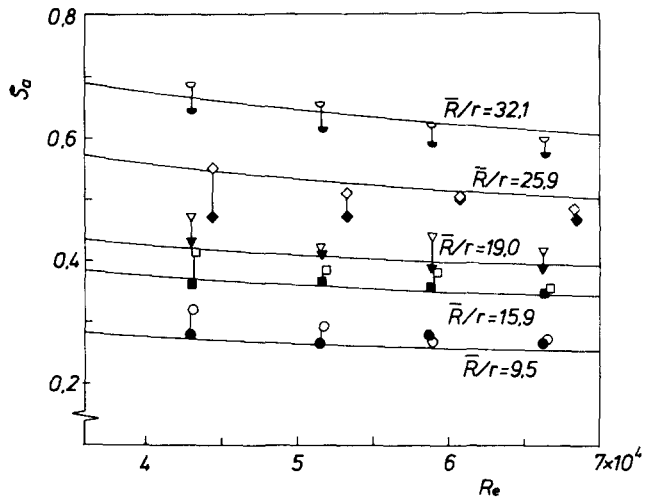

Figure 5. Coefficient of pressure drop due to the elliptical bend: ——, Itō's formula [9]. For legend see figure 9.

curvature representing the bend, $\bar{R}$, is an average obtained by dividing the bend length by the turning angle. It is found from the figure that Itō's formulae are also applicable to the elliptical bend if the average curvature ratio mentioned above is substituted. Observing the figure in detail, however, the case where a long sweep is at the upstream end seems to give a slightly lower value than the opposite case.

5. ADDITIONAL PRESSURE DROP DUE TO THE PARTICLES

Straight pipe

The additional pressure drop in the constant velocity region are discussed first. Figure 6 shows the coefficient of additional pressure drop defined by [5], in which measurements in both the upstream and downstream sections are given. The coefficient λ_s is independent of the air velocity larger than 20 m/s. The relationship between the coefficient λ_s and the loading ratio n can be approximated by a straight line, although the measurements in the downstream section scatter somewhat largely.

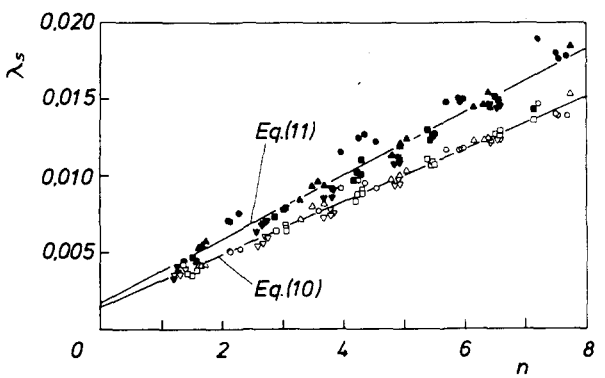

Figure 6. Relation between the coefficient of additional pressure drop, λ_s, and the loading ratio, n. In the straight pipe:

upstream	downstream	u m/s
○,	●,	18
△,	▲,	22
□,	■,	26
▽,	▼,	29.

$$\lambda_s = (1.51 + 1.69n) \times 10^{-3} \text{ upstream,} \quad [10]$$

and

$$\lambda_s = (2.06 + 1.75n) \times 10^{-3} \text{ downstream.} \quad [11]$$

The extrapolation of the straight pipe data does not pass through the origin of the figure. Some results by earlier investigators show the same deviation as the present one, but others do not. The reason for this deviation is not well understood in the present work. In addition to the deviation, the figure indicates that λ_s shows a higher value in the downstream than in the upstream section. This is attributable to the fact that even in the most downstream section the particles were still accelerating and thus λ_s includes a small component of the pressure drop for particle acceleration. This result is very meaningful in discussing the accuracy of earlier experiments concerned with the bend. The particles used in the present experiment have the terminal velocity of 4.1 m/s, and need a distance of more than $240D$ to reach the constant velocity region after the bend. Many earlier experiments used larger particles such as various kinds of granular materials. In most of those experiments, the range of measuring sections was within $100D$ after the bend. Therefore, so long as the definition about the pressure drop due to the bend is based on the pressure difference Δp_b in figure 3, it is possible that the results of those works include quantitatively large errors.

Circular bend

Figure 7 shows the coefficient of additional pressure drop defined by [8]. As is different from figure 6, the coefficient ζ_s depends largely on the air velocity. Here an empirical formula which approximates the present results of ζ_s is constructed by refering to the formulae by earlier investigators.

Schuchart (1968) considered the ratio of the pressure drop due to the bend to the pressure drop in the straight pipe. His formula can be expressed using the coefficients ζ_s and λ_s as follows:

$$\zeta_s/\lambda_s = 165(R/r)^{-0.15}. \quad [12]$$

According to Ikemori & Munakata (1973), ζ_s/λ_s is inversely proportional to Froude number F_r ($= u/\sqrt{gD}$). While the coefficient λ_s is independent of the air velocity, the coefficient ζ_s depends on it even in the same range of air velocity as shown in figure 7. Therefore, Schuchart's formula which does not include F_r is not fit to the present results. However, with respect to the effect of R/r, his formula shows the same tendency as the present results. Hence, refering to [12] and assuming that ζ_s/λ_s is inversely proportional to F_r, a new empirical expression is made.

Figure 8 shows the relation between $\zeta_s F_r/\lambda_s$ and R/r, where λ_s is the value for the upstream

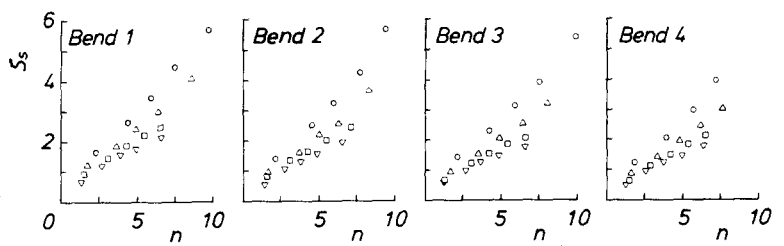

Figure 7. Relation between the coefficient of additional pressure drop due to the bend, ζ_s, and the loading ratio, n.

u m/s
○, 18
△, 22
□, 26
▽, 29.

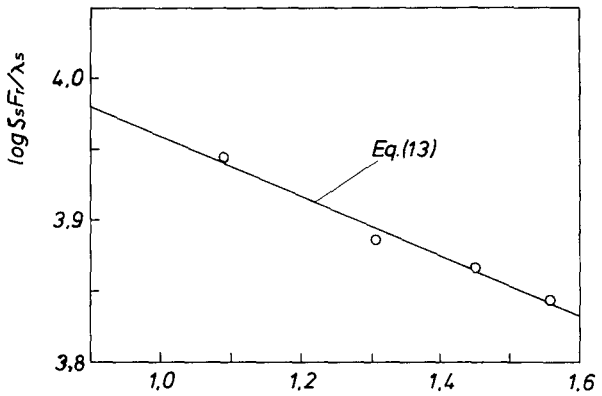

Figure 8. Relation between $\zeta_s F_r/\lambda_s$ and curvature ratio, R/r circular bend.

straight pipe. The plotted values are those averaged from the measurements of $n = 1$ to 8. From the figure, the following equation can be proposed:

$$\frac{\zeta_s}{\lambda_s} = \frac{1.5 \times 10^4}{F_r(R/r)^{0.2}}, \quad F_r > 30. \qquad [13]$$

Although the constant in the numerator in [13] is considered to depend on the properties of particles such as the terminal velocity, one cannot know the dependence from the present work using the only one kind of particle. In order to obtain the pressure drop due to the bend correctly for the particles with larger terminal velocities, the pipe distance before and after the bend must be made longer in the experiment.

Elliptical bend

Also in the case of the elliptical bend, the relation between ζ_s and n showed the qualitatively same trend as that of the circular bend. Thus, according to the same procedure as in the last section, the measured results were studied. As the curvature representing the elliptical bend, the average curvature $\bar{R}$ defined in section 4 was adopted first, and the relation between $\zeta_s F_r/\lambda_s$ and $\bar{R}/r$ was plotted in figure 9. The solid line in the figure represents [13]. Like the case of the

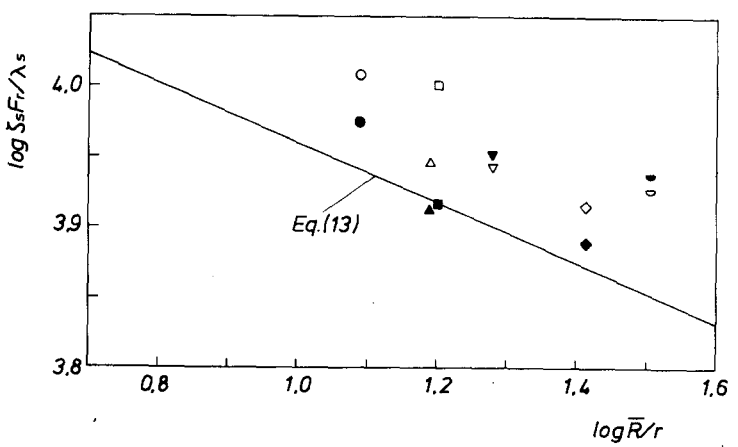

Figure 9. Relation between $\zeta_s F_r/\lambda_s$ and curvature ratio, R/r elliptical bend.

○, 5 □, 7 ◇, 9
●, 5′ ■, 7′ ◆, 9′
△, 6 ▽, 8 ⬭, 10′
▲, 6′ ▼, 8′ ⬬, 10′

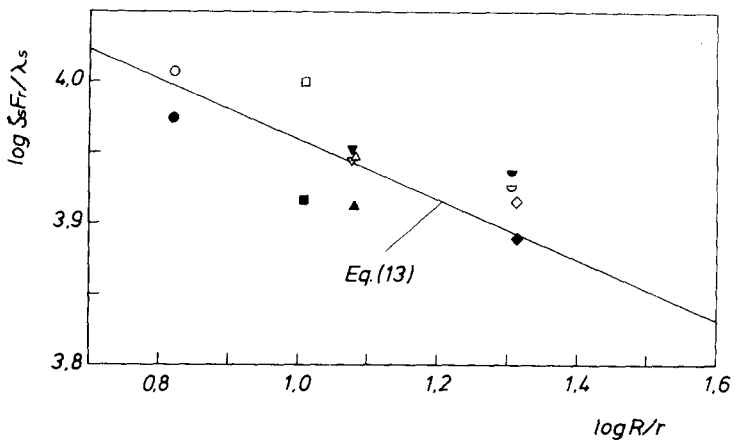

Figure 10. Relation between $\zeta_s F_r/\lambda_s$ and curvature ratio, R/r elliptical bend. For legend see figure 9, R corresponds to short radius.

circular bend, the value of $\zeta_s F_r/\lambda_s$ decreases with increasing $\bar{R}/r$, and the bend with a long sweep at the upstream and a short radius at the downstream end gives a slightly smaller value. Making a comparison of measurements with [13], one finds that the measurements generally show higher values than the equation. Thus, as an attempt, the same data are replotted in figure 10 using the curvature of short radius instead of the average one for the abscissa. The figure shows that agreement between measurements and [13] is improved, although the data scatter around [13] to some extent. Therefore, with respect to the additional pressure drop, the elliptical bend is found to be equivalent to the circular bend, if the curvatures of a short radius are used as the representative curvatures. This result is different from the case of a single phase flow, where the average curvature $\bar{R}$ is representative for the pressure drop. The additional pressure drop due to the bend corresponds to the kinematic energy that the particles lose within the bend. The foregoing results mean that in the case of elliptical bend, the place with the sharpest curvature is most critical for this energy loss.

6. CONCLUSIONS

The pressure drop due to the horizontal 90° circular and elliptical bends were measured for single phase and air–solids two-phase flows. The results are:

1. In a single phase flow, the pressure drop due to the elliptical bend agrees with Itō's formulae for the circular bend, if the average curvature is substituted into the formulae.
2. In an air–solids two-phase flow, the additional pressure drop due to the elliptical bend agrees with the results of the circular bend, of which curvature corresponds to a short radius of the elliptical bend.
3. When the elliptical bend is constructed with a long sweep at the upstream and a short radius at the downstream, the pressure drop is slightly smaller than the inverse setting, in both single and two phase flows.
4. An empirical formula for the additional pressure drop due to the bend was derived by taking the Froude number and curvature ratio into account.

Acknowledgement—This work was supported by the Scientific Research Fund of the Japan Ministry of Education.

REFERENCES

IKEMORI, K. & MUNAKATA, H. 1973 A new method of expressing pressure drop in horizontal pipe bend in pneumatic transport of solids. *Proc. Pneumotransport* 2, BHRA, A3–33.

ITŌ, H. 1960 Pressure losses in smooth pipe bends. *Trans. Am. Soc. Mech. Engrs (J. Bas. Engng)* **82D**, 131–143.

SCHLICHTING, H. 1968 *Boundary Layer Theory*, 6th Ed. (Trans., J. Kestin), p. 561. Pergamon, Oxford.

SCHUCHART, P. 1968 Widerstandsgesetze beim pneumatischen Transport in Rohrkrümmern. *Chemie-Ing.-Tech.* **40**(21/22), 1060–1067.

ZENZ, F. A. & OTHMER, D. F. 1960 *Fluidization and Fluid–Particle Systems*, p. 338. Reinhold.